



Geochemistry, Geophysics, Geosystems



RESEARCH ARTICLE

10.1029/2022GC010353

Key Points:

- Ancient melt depletion can be preserved despite metasomatism and suggest Ferrel Seamount peridotite was formed by mid-ocean ridge processes
- Ferrel Seamount peridotites likely represent preserved Pacific-Farralon lithosphere
- A tectonic process, ridge jump, can isolate oceanic lithosphere and provides a starting point for the formation of continental lithosphere

Supporting Information:

Supporting Information may be found in the online version of this article.

Correspondence to:

B. Oller, boller@ucsd.edu

Citation:

Oller, B., Day, J. M. D., Driscoll, N. W., & Lonsdale, P. F. (2022). Generation of continental lithospheric mantle by tectonic isolation of oceanic plate. *Geochemistry, Geophysics, Geosystems*, 23, e2022GC010353. https://doi.org/10.1029/2022GC010353

Received 21 JAN 2022 Accepted 3 OCT 2022

© 2022. The Authors. This is an open access article under the terms of the Creative Commons Attribution License, which permits use, distribution and reproduction in any medium, provided the original work is properly cited.

Generation of Continental Lithospheric Mantle by Tectonic Isolation of Oceanic Plate

Brian Oller¹, James M. D. Day¹, Neal W. Driscoll¹, and Peter F. Lonsdale¹

¹Scripps Institution of Oceanography, University of California San Diego, La Jolla, CA, USA

Abstract Continental formation models invoke subduction or plume-related processes to create the buoyant, refractory character of continental lithospheric mantle (CLM). From similarities in melt depletion, major element composition, modal clinopyroxene, and Os isotope systematics it has been proposed that oceanic mantle lithosphere is the likely protolith to non-cratonic CLM, however, a direct link between the two has been difficult to ascertain. Using dredged mantle peridotite xenoliths from the Ferrel Seamount, off the west coast of Baja California, Mexico, we show that tectonic isolation of an oceanic plate may lead to formation of non-cratonic CLM. Ferrel xenoliths are coarse-grained spinel lherzolite, or rare harzburgite. Bulk-rock and clinopyroxene trace element compositions reveal two-stages of melt refertilization following melt depletion, with infiltration by mid-ocean ridge basalt-type melts, followed by melt addition from host alkali basalt. Melt depletion correlations with ¹⁸⁷Os/¹⁸⁸Os and highly siderophile element abundances indicate preserved melt depletion and refertilization processes are ancient. From these observations, the Ferrel xenoliths represent lithosphere from the abandoned Pacific-Farallon ridge. The history of melt depletion, followed by MORB-melt refertilization is consistent with the peridotites representing oceanic mantle lithosphere that was subsequently incorporated into the Baja-Guadalupe microplate during "ridge jump." These peridotites demonstrate that isolation of oceanic lithosphere that is rafted onto a continental margin provides a viable means for producing non-cratonic CLM. We suggest that continuation of late-stage, low degree melt refertilization may provide a link between oceanic lithosphere and non-cratonic CLM and propose a tectonic model to preserve and facilitate this continued evolution.

1. Introduction

The formation of thick, geologically stable non-cratonic continental lithospheric mantle is partially responsible for the oceanic-continental crustal dichotomy, and is fundamental for the formation of continents beyond the cratons (Pearson & Wittig, 2008; Pearson et al., 2021). Despite the relative importance of continental lithospheric mantle, the mechanisms of its formation remain poorly understood. Several hypotheses have been outlined, all involving substantial melt extraction of mantle residues either by deep plume melting (Boyd, 1989; Griffin et al., 1998), shallow melting and subduction (e.g., Canil & Wei, 1992; Schulze, 1986), or by lithospheric melt extraction prior to subduction stacking (Canil, 2004; Lee, 2006; Simon et al., 2008). Furthermore, the mechanisms by which continental lithosphere has formed may have changed with time, as mantle potential temperatures have decreased since the Archean (e.g., Nisbet et al., 1993), and progressive Wilson cycles have occurred (Shirey & Richardson, 2011).

Understanding of the nature of the non-cratonic continental lithospheric mantle (CLM) has been predominantly driven by studies of mantle xenolith suites, where peridotite nodules are entrained in alkali basalts, basanites and other low degree partial melts, during magma ascent to the surface (e.g., P. N. Nixon, 1987). In these cases, melt depletion trends can be well-preserved in peridotite xenolith suites (e.g., Frey & Green, 1974; Frey & Prinz, 1978; Galer & O'Nions, 1989; Jagoutz, 1988) in spite of metasomatic effects. Oceanic lithosphere shows melt depletion trends with variable degrees of refertilization, but the effects of most melt refertilization can be decoupled from primary melt depletion trends (Day et al., 2017; Niu, 2004). In contrast, the CLM has a prolonged history of exposure to variable degrees of depletion and refertilization (Galer & O'Nions, 1989; Pearson et al., 1995). The different melt depletion/refertilization histories of CLM and oceanic mantle lithosphere can generally be attributed to the isolation of CLM from subduction, removing it from recycling and mixing processes in the mantle.

Abyssal peridotites are compositionally distinct from non-cratonic CLM peridotites, but broad overlap of the two mantle domains suggests a common link, with CLM formed from upper mantle materials over Earth history. For

OLLER ET AL. 1 of 15

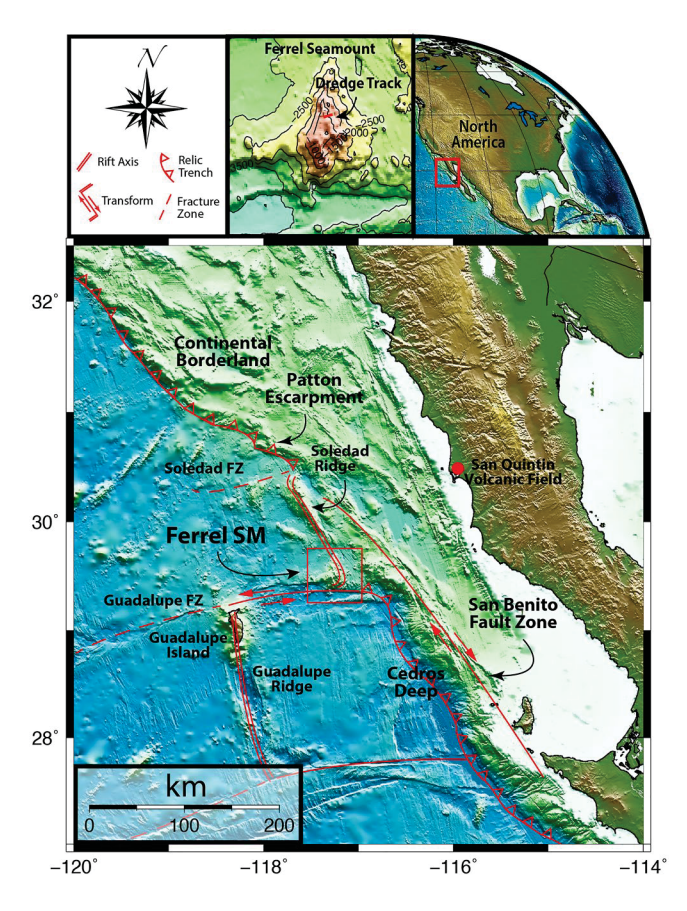


Figure 1. Regional bathymetry and elevation model map for offshore northern Baja California, Mexico. Highlighted is the Ferrel Seamount (topographic map, 500 m intervals) with the red box showing the location of the WOBA-3D dredge track. This locality sits atop an abandoned section of East Pacific/ Farallon Rise, known as the Soledad Ridge (Lonsdale, 1991).

example, globally, CLM is often indistinguishable from oceanic lithosphere in terms of degree of melt extraction, bulk rock and mineral Mg/Fe ratios, and stabilization model ages (Pearson et al., 2004 and Supporting Information S1). This is in strong contrast with on-craton mantle xenoliths that are highly depleted with Proterozoic or Archean model ages. These similarities have led some authors to postulate oceanic lithosphere as a potential protolith for the non-cratonic CLM (i.e., Harvey et al., 2012; Peslier et al., 2000). While similarities exist, differences in fundamental constituents such as major element composition, and modal clinopyroxene content require additional processes in their genesis. Abyssal peridotites are typically represented by spinel facies lherzolites and harzburgites that have experienced ≤20% melt extraction, with long-term stability compared to oceanic lithosphere being a key feature of CLM (Lassiter et al., 2014; Pearson et al., 1995). The distinction in age also implies the older CLM has been exposed to refertilization from percolating melts for a longer period than for abyssal peridotites. If CLM can form from oceanic lithosphere in the present-day it must be tectonically isolated to a continental margin, as the clear majority of oceanic lithosphere is recycled within subduction zones (e.g., Stern, 2002).

Here, we consider the geochemical and tectonic implications of spinel peridotite xenoliths dredged from the Ferrel Seamount offshore Baja California for the formation of recent CLM. The xenoliths come from an isolated microplate formed during the subduction to rift transition and southern migration of the Rivera triple junction, ~10 to ~14 Ma, along the Pacific and North American plate boundary (Lonsdale, 1991). New major and trace element abundance data are compared to bulk rock and mineral highly siderophile element concentrations (HSE; Os, Ir, Ru, Pt, Pd, Re) and 187Os/188Os data of non-cratonic CLM-derived xenoliths from the southwest USA (Dish Hill, CA and Kilbourne Hole, NM; Armytage et al., 2014; Harvey et al., 2012). Effects of refertilization on young, buoyant oceanic lithosphere are examined and compared to the known geochemistry of peridotites at CLM localities. The results of our study reveal the melt depletion and refertilization process on the abandoned Pacific-Farallon ridge, confirming the conclusions of previous studies of HSE abundance and ¹⁸⁷Os/¹⁸⁸Os systematics for abyssal peridotites (Brandon et al., 2000; Day et al., 2017; Harvey et al., 2006; Warren, 2016),

and imply an oceanic lithosphere protolith. Comparison of Ferrel Seamount with western United States xenolith suites indicates that formation of some recent non-cratonic CLM may have begun when the oceanic fragment was "welded" to the over-riding plate after ridge jump.

2. Geological Setting and Samples

The Ferrel Seamount (29° 33.90°N, 117° 15.60°W) is located off the west coast of Baja Mexico, between Guadalupe Island to the west and the San Quintin volcanic field to the east. The seamount was constructed from mafic to intermediate alkali lavas and intrusive units that were probably emplaced at an abandoned Pacific-Cocos spreading center (Lonsdale, 1991) (Figure 1). The Ferrel Seamount lies on the western boundary of a section of crust formed at the abandoned East Pacific Rise and the southern boundary of an associated transform fault, the Guadalupe Fracture Zone. The north-northwestern boundary abuts the southern extent of the Patton Escarpment. Although tectonic deformation from the southern Continental Borderlands, as well as terrigenous sediment partially obscure the magnetic anomalies proximal to the Ferrel Seamount, resolution of Chron 5AC provides an estimated crustal age of ~10~14 Ma (Müller et al., 2008). Samples investigated here were collected during the WOBA-3D dredge from the Ferrel Seamount in October 2012, aboard R/V Melville. The WOBA-3D dredge recovered >200 kg of material, including alkali basalt lavas containing fresh spinel peridotite xenoliths and at least one gabbro xenolith, at an average water depth of 800 m (Figure 1).

OLLER ET AL. 2 of 15

l5252027, 2022, 11, Downloaded from https://agupubs.onlinelibrary.wiley.com/doi/10.1029/2022GC010353 by University Of California,

Wiley Online Library on [11/07/2024]. See the Terms and Conditions (https://

3. Analytical Methods

Fourteen spinel peridotite xenoliths, one gabbro xenolith, and three lava samples were selected from a larger sample suite. The xenoliths are roughly elliptical ranging in size from ~10 to 16 cm across the long axis and ~5–8 cm across the short axis with weights ranging from ~0.5 to ~10 kg. Major-element mineral chemistry was determined with a *Cameca SX-100* electron probe micro analyzer at the University of Tennessee. Modal abundances were determined through photo analysis of thin sections and cut slabs as well as quantitatively based on mineral major element compositions using the constrained least squares method described in Albarède (1995). Trace-element abundances in minerals were obtained using a *New Wave Research UP213* (213 nm) laser-ablation system coupled to a *ThermoScientific* iCAPQ c ICP-MS at the *Scripps Isotope Geochemistry Laboratory (SIGL)* with standardization performed relative to standard reference material glasses NIST 610, BCR-2G and BHVO-2G for silicate minerals and MASS-1 sulfide and iron meteorite metals for sulfides (Jochum et al., 2005).

For whole-rock compositions, powders were measured for major element compositions by X-ray fluorescence (XRF) at Franklin and Marshall College using a *PW 2404 PANalytical* XRF vacuum spectrometer. Trace-element abundances were determined at the *SIGL* using a *ThermoScientific* iCAPQ c ICP-MS. Reproducibility of the reference materials was generally better than 5% (RSD) for basaltic and peridotite standards. Osmium isotopes and HSE (Re, Pd, Pt, Ru, Ir, Os) abundances were determined using isotope dilution at the *SIGL*. Osmium was triply extracted using CCl₄, back-extracted into HBr and purified by micro-distillation. Rhenium and platinum group elements were recovered and purified from the residual solutions by anion exchange separation, and then analyzed on a *ThermoScientific* iCAPQ c ICP-MS. Isotopic compositions of Os were measured in negative-ions using a *ThermoScientific* Triton thermal ionization mass spectrometer. Total procedural blanks typically represented <5% of total analyte with the exception of Re and Pd, which were <16% in the worst cases. Detailed analytical methods are provided in the Supporting Information S1 accompanying this article.

4. Results

4.1. Textures, Modal Mineralogy, and Mineral Compositions

Peridotites from the Ferrel Seamount have coarse, equigranular textures and are dominantly spinel lherzolites (43.7–68.2 modal % olivine; 17.5 to 40.8 modal % orthopyroxene; 20.0 to 8.7 modal % clinopyroxene; 0.6 to 3.2 modal % spinel), with one spinel harzburgite, WOBA-3D-5 (68.8 modal % olivine; 24.3 modal % orthopyroxene; 3.2 modal % clinopyroxene; 3.8 modal % spinel). Using the constrained least squares approach of Albarède (1995) yields tighter ranges of olivine and pyroxene modal mineralogy, and slightly overestimates spinel relative to the optical mode (60.8–64.3 modal % olivine; 21.3 to 26.7 modal % orthopyroxene; 9.3 to 11.2 modal % clinopyroxene; 1.6 to 3.5 modal % spinel). The disparity between the two methods is likely a result of disequilibrium between the pyroxene phases, where the quantitative model assumes equilibrium between the two. Both intra-granular Type 1 and interstitial Type 2 sulfide phases, as defined by Luguet and Pearson (2019), are represented in the sample set. Interstitial Type 2 elongated skeletal grains are less than 10 microns across, while Type 1 have intra-granular rounded to sub-rounded sulfide grains, hosted primarily in orthopyroxene. The extent of melt glass infiltration is limited to the outer periphery of xenolith samples, where little evidence of melt reaction with adjacent minerals was observed. Olivine compositions from the xenoliths have Mg-numbers from 84.7 to 91.8. Orthopyroxene has enstatite composition ($En_{0.888\pm0.008}Wo_{0.017\pm0.003}Fs_{0.095\pm0.007}$), with Mg-numbers from 89.2 to 91.9. Clinopyroxene is homogeneous Cr-diopside ($En_{0.486\pm0.006}$ $Wo_{0.467\pm0.009}$ $Fs_{0.047\pm0.004}$), with Cr₂O₃ from 0.7 to 1.3 wt. %, and Mg-numbers between 91.2 and 89.9. Spinel Mg-numbers from 66.0 to 73.5 (70.6 ± 2.3) and Cr-numbers from 18 to 40.3 (25.2 ± 5.7) , falling within the compositional field of abyssal peridotites (Figure 2), and corresponding to between 7% and 15% melt depletion using the method of Hellebrand et al. (2001), with an average of $10 \pm 2\%$.

Orthopyroxene grains in the Ferrel Seamount samples typically have lower absolute abundances ($<0.1 \times PM$) of the incompatible trace elements than depleted mid ocean ridge basalt mantle (DMM) estimates (Workman & Hart, 2005), but they have systematically higher La, Ba and Rb (Figure 3a). Like DMM orthopyroxene compositions, and orthopyroxene grains measured from the Gakkel Ridge (D'Errico et al., 2016), Ferrel Seamount xenoliths contain orthopyroxene grains with large Zr and Hf enrichments relative to elements of similar incompatibility. Unlike DMM, however, the Ferrel Seamount samples do not have prominent Nb or Ta enrichments in orthopyroxene. Clinopyroxene grains generally have lower abundances of the incompatible trace elements

OLLER ET AL. 3 of 15

15252027, 2022, 11, Downloaded from https://agupubs.onlinelibrary

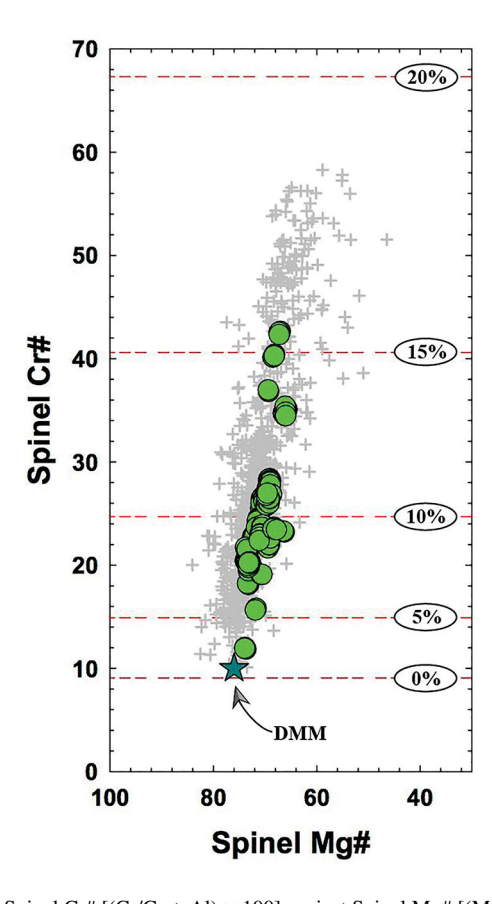


Figure 2. Spinel Cr# [(Cr/Cr + Al) \times 100] against Spinel Mg# [(Mg/Mg + Fe) \times 100] for Ferrel Seamount peridotites (green circles) versus a "global field" of abyssal peridotites (gray crosses; from Warren [2016] and references therein). Depleted MORB Mantle (blue star) from Workman and Hart (2005). Melt removal lines (red dashed lines) are from Hellebrand et al. (2001).

(<1 × PM) than DMM (Figure 3b). The patterns for clinopyroxene exhibit a notable variation in the LREE, where La/YbPM and Sm/YbPM span a range of values from 0.06 to 1.6 and 0.06 to 1.7, respectively.

4.2. Bulk-Rock Major and Trace Element Compositions

Ferrel Seamount xenoliths are generally extremely fresh peridotites characterized by low bulk-rock Al₂O₃ (1.06-2.59 wt. %) and CaO contents (0.75–3.03 wt. %). The MgO-Al₂O₃-SiO₂ systematics of the xenoliths indicate greater depletion than non-cratonic CLM xenolith suites, such as Dish Hill, or Kilbourne Hole (Figure 4), plotting between the mean composition of cratonic and non-cratonic peridotite xenoliths (Pearson et al., 2004). Magnesium-numbers for samples range between 88 and 90.7, within the off-craton range (Pearson et al., 2004). Ophiolitic terranes may have formed in supra-subduction settings, and so likely experienced modification from slab de-watering (i.e., Choi et al., 2008; Snortum & Day, 2020) thus, we limit the comparison to peridotite xenoliths. Using the two-pyroxene and calcium orthopyroxene thermobarometers of Brey and Köhler (1990), equilibration temperatures range from 887 to 1061°C and 932-1069°C respectively, at a reference pressure of 2 GPa, at the extent of spinel stability. Average log fO₂ Δ QFM was estimated in a range of +0.4 to +1.4 for the sample set, at the upper range of abyssal peridotites. The peridotite xenoliths have relatively homogeneous abundances of Cr (2,500 \pm 300 ppm), Ni (2,100 \pm 140 ppm), Ti (220 \pm 90 ppm), Li (1.0 \pm 0.2 ppm), Sc (11 \pm 3 ppm), V (52 \pm 12 ppm), Co (99 \pm 5 ppm), Cu (5 \pm 3 ppm), and Zn (33 \pm 4 ppm). The xenoliths show a wide range in both absolute ($\sim 0.06-1 \times PM$) and relative (La/Yb = 0.7 to 3.7) incompatible trace element abundances, with relative enrichments in Ba, U, Zr and Hf, and relative depletions in Pb and K (Figure S1 in Supporting Information S1). Samples WOBA-3D-10, and -17 both have prominent Zr and Hf enrichments relative to the sample suite; this is likely the effect of trace-element enriched infiltrated glass observed in the two samples (Figures S1 and S3 in Supporting Information S1).

The host lavas are alkali basalts with high MgO (12.3 \pm 1.2 wt.%) and are incompatible element enriched patterns (~4-100 \times primitive mantle). A

single gabbro xenolith has a composition similar to mid-oceanic ridge gabbros (Niu & O'Hara, 2003) with high Al_2O_3 and CaO and flat primitive mantle normalized incompatible trace element pattern (Figure S2 in Supporting Information S1, see Supporting Information S1 for detailed descriptions).

4.3. Highly Siderophile Element Abundances and ¹⁸⁷Os/¹⁸⁸Os

Highly siderophile element abundances (HSE: Re, Pd, Pt, Ru, Ir, Os) for Ferrel Seamount peridotites are similar to those of East Pacific Rise abyssal peridotites (Paquet et al., 2022; Rehkämper et al., 1999), with variable depletions in Re and Pd relative to Pt, Ru, Ir, and Os (Table 1). Absolute and relative abundances of Os, Ir, and Ru (Os/ Ir = 0.86 ± 0.19 ; Ru/Ir = 2.15 ± 0.29) from the Ferrel Seamount are consistently depleted relative to Primitive Mantle (PM) estimates (Day et al., 2017). In contrast, Pd and Pt abundances exhibit considerable dispersion (Pd/ Ir = 1.42 ± 0.68 ; Pt/Ir = 2.01 ± 0.64), with absolute Pd abundances that range from ~ 0.04 – $1.2 \times$ PM. Absolute abundances of Re span a wider range of depleted values (0.04– $0.9 \times$ PM), and produce a broad variation or "fanning" pattern (Re/Ir = 0.03 ± 0.02) (Figure 5). The HSE are poorly correlated with bulk rock melt depletion indicators (i.e., MgO, Al_2O_3), except for Re, which approximately co-varies with MgO (r^2 = 0.55).

The $^{187}\text{Os}/^{188}\text{Os}$ ratios measured in the bulk-rock peridotite xenoliths range from 0.1170 to 0.1326, consistent with the range in $^{187}\text{Os}/^{188}\text{Os}$ for off-craton xenoliths from the western United States (Armytage et al., 2014; Harvey et al., 2012; Meisel et al., 2001), and corresponds to averages for abyssal peridotites proposed by Lassiter et al. (2014) (0.1263 \pm 0.0099, 2 SD) and Day et al. (2017) (0.1275 \pm 0.0153, 2 SD). Applying the Os isotope

OLLER ET AL. 4 of 15

15252027, 2022, 11, Downloaded from https://agupubs.onlinelibrary.wiley.com/doi/10.1029/2022GC010353 by University Of California, Wiley Online Library on [11/07/2024]. See the Terms

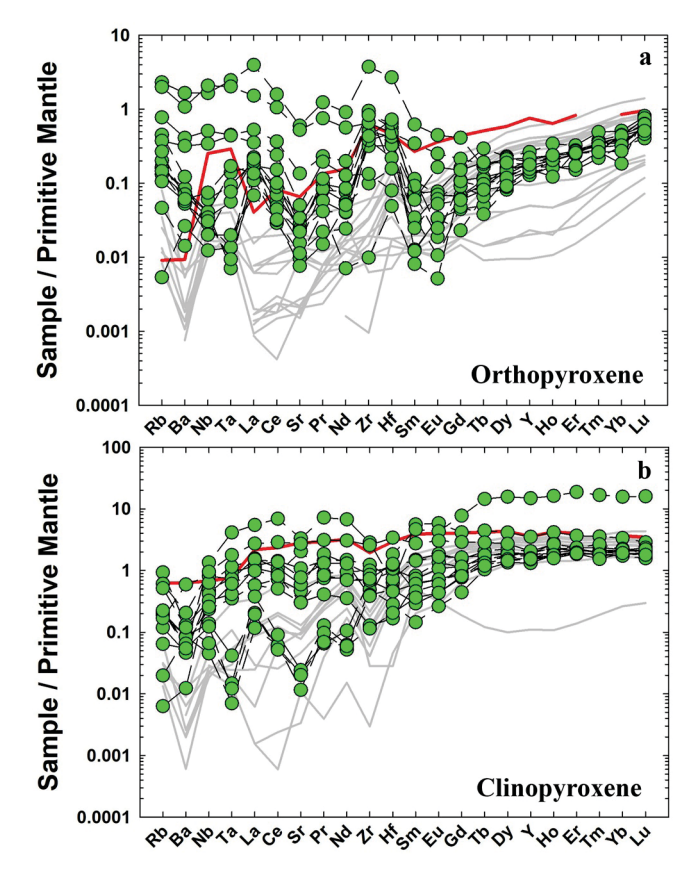


Figure 3. Primitive mantle normalized trace element patterns for (a) orthopyroxene and (b) clinopyroxene grains (green circles with dashed lines) from Ferrel Seamount peridotites. Depleted MORB Mantle (thick red line) (Workman & Hart, 2005), and (gray lines) Gakkel Ridge (a) orthopyroxene, and (b) clinopyroxene grains from D'Errico et al. (2016) are shown for comparison. Primitive mantle normalization is given in the Supporting Information S1.

ratios of Ferrel Seamount peridotites to model ages of Re depletion gives an average age of 0.73 \pm 0.49 Ga, with individual $T_{\rm RD}$ ages up to 1.8 Ga. These model ages correspond with the distribution of Nd model ages for abyssal peridotites proposed by Mallick et al. (2014) (<2.4 Ga). The sample suite shows a rough correlation in $^{187}{\rm Re}/^{188}{\rm Os}^{-187}{\rm Os}/^{188}{\rm Os}$ space but does not define an isochronous relationship, whereas $^{187}{\rm Re}/^{188}{\rm Os}$ and $^{187}{\rm Os}/^{188}{\rm Os}$ ratios correlate negatively with bulk rock MgO ($r^2=0.64;\,0.51$), and positively with bulk rock Al $_2{\rm O}_3$ ($r^2=0.62;\,0.48$) (Figure S6 in Supporting Information S1).

5. Discussion

The new data for Ferrel Seamount peridotites and their similarity to oceanic abyssal peridotites, along with the tectonic framework in which the xenoliths occur, after ridge jump and plate isolation, suggest a possible link between oceanic and continental lithospheric mantle. In the following discussion, we consider the possible effects of tectonic isolation, metasomatism, melt refertilization and melt depletion, ultimately establishing hypotheses for non-cratonic CLM formation.

5.1. Metasomatic Processes Affecting Ferrel Seamount Peridotites

Metasomatism by melts of variable compositions is a common characteristic of abyssal peridotites (e.g., D'Errico et al., 2016; Warren, 2016). Notable geochemical evidence in the Ferrel Seamount peridotites are the elevated relative abundances of incompatible trace elements within whole-rock samples that are not reflected in clinopyroxene, the main carrier of the LREE in peridotites (Figure S1 in Supporting Information S1; Figures 6a and 6b). Eight of the 14 peridotite samples have whole-rock (La/Yb) $_{\rm N}$ > 1 (WOBA-3D-1, -3, -5, -6, -10, -12, -17, -31) indicating that the LREE were added by interaction with migrating melts (e.g., Johnson et al., 1990). The remainder of the samples (WOBA-3D-7, -9, -11, -14, -15, -32) have U-shaped REE patterns with (La/Yb) $_{\rm N}$ near unity, suggesting depletion of LREE–MREE followed by cryptic metasomatic addition, resulting in the enrichment of light REE, relative to primitive mantle, in the bulk rock.

LREE enrichments relative to the HREE in peridotites can only be achieved through reaction with small melt volumes (D'Errico et al., 2016; Hellebrand, 2002). To test this hypothesis on Ferrel Seamount peridotites samples we used a closed system equilibrium model starting with the most REE depleted Ferrel peridotite sample, WOBA-3D-14 and incrementally added the alkali host rock composition ((La/Yb)_N = 12.9 \pm 1) (Figure 7). The results demonstrate that ~0.1%-1.5% addition of this melt can approximate the REE range of the Ferrel Seamount peridotites. The LREE in whole-rock peridotites are therefore sensitive tracers of melt modification that are otherwise unrecognized from mineralogical or textural attributes in samples. Such cryptic metasomatism likely results from re-equilibration at mantle temperatures, consistent with both our results and those of previous studies (e.g., D'Errico et al., 2016; Harvey et al., 2012; Hellebrand, 2002).

Melt refertilization processes are also evident from clinopyroxene grains in Ferrel Seamount peridotites. Clinopyroxene grains have 120° triple junctions, exsolution lamellae of clinopyroxene from orthopyroxene, and vermicular spinel, possibly consistent with garnet breakdown textures, implying long-term equilibration at high temperature (Figure S3 in Supporting Information S1). The clinopyroxene grains have elevated incompatible trace element and LREE relative abundances (Figures 6a and 6b). Our results support previous suggestions that clinopyroxene grains hosted in spinel peridotites are not a primary phase, but resulted from melt refertilization, or were exsolved from orthopyroxene and/or garnet (e.g., Johnson et al., 1990; Niu, 2004).

The LREE enrichment apparent in the whole-rock REE patterns in conjunction with the exsolution textures and incompatible REE enrichments of clinopyroxene suggest at least two episodes of melt refertilization. First, from a

OLLER ET AL. 5 of 15

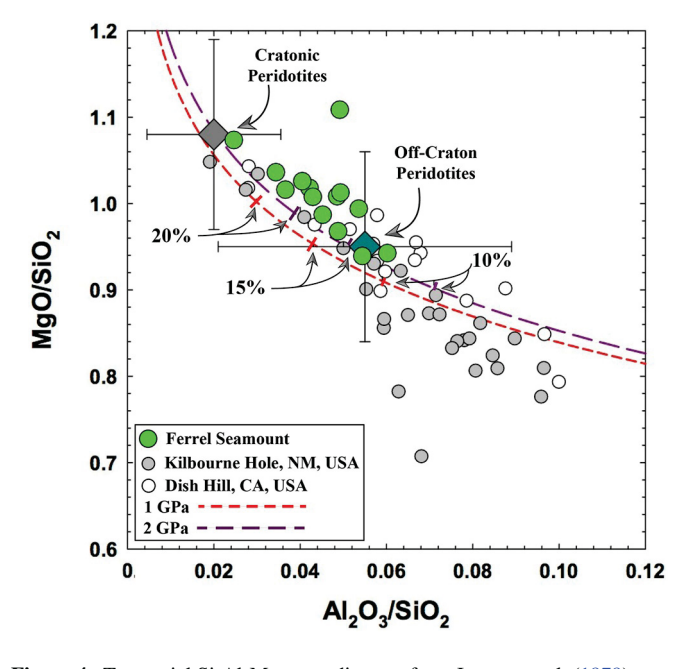


Figure 4. Terrestrial Si-Al-Mg array diagram from Jagoutz et al. (1979), with melting curves at 1 and 2 GPa from Herzberg (2004). Filled diamonds represent the average compositions of cratonic and non-cratonic peridotites (Pearson et al., 2004). Calculated melt depletion percentages (bold tick marks) are annotated on the figure.

tholeiitic MORB-like melt during interaction of Ferrel Seamount peridotites at a mid-ocean ridge. This is likely responsible for the textural observations in clinopyroxene grains. Second, low-degree, alkali basalt melt refertilization evidenced by elevated whole-rock LREE's imparted as cryptic metasomatism. Melt refertilization episodes have also likely affected the main HSE host sulfide populations in the peridotites. Ferrel Seamount peridotites can be broken into two groups based on the sulfide population classifications of Luguet and Pearson (2019), those with rounded intra-granular sulfides hosted primarily in orthopyroxene (Type 1), and those predominantly hosting interstitial sulfides (Type 2). Twelve sulfide grains were analyzed from five samples, WOBA-3D-05, -10, -12, -17, and -31. Of those sulfides, five are classified as Type 1, and seven as Type 2 (Figures S4 and S5 in Supporting Information S1). Harvey et al. (2006) have demonstrated that interstitial sulfides in the abyssal peridotites that they studied were a metasomatic product precipitated from sulfide-rich melts. Because sulfides exist at grain boundaries they are susceptible to open system behavior by precipitation of Re and Pd from low degree sulfide rich melts (Luguet et al., 2003). Ferrel Seamount peridotites exhibit highly variable Re and Pd contents, but inter-element HSE ratios of the Ferrel peridotites are approximately chondritic, indicative of minor refertilization following melt depletion (Rehkämper et al., 1999). Therefore, despite evidence for formation of interstitial sulfides during refertilization (e.g., Luguet & Reisberg, 2016), the overall tenor of HSE compositions in the Ferrel Seamount peridotites appears to have been largely unaffected by these processes, and instead indicates progressive decrease in Pd/Ir with increasing degrees of partial melt loss (Figure 8).

5.2. HFSE Fractionation in Pyroxene Grains

Fractionation patterns of the high field strength elements (HFSE: Nb, Ta, Zr, and Hf) in Ferrel Seamount peridotite pyroxene grains show considerable variability relative to the whole-rock, suggesting a complex history of depletion and re-fertilization typical of spinel facies mantle peridotites (e.g., Niu, 2004; Pfänder et al., 2007; Rudnick et al., 1993; Weyer et al., 2003). The elemental pairs Nb-Ta and Zr-Hf have the same charge (5+ and 4+ respectively), similar ionic radii, and peridotite-melt distribution coefficients (~0.5), therefore the initial ratios of Nb/Ta and Zr/Hf should remain relatively constant during a single melting event (Pearce & Parkinson, 1993). However, the HFSE ratios from orthopyroxene and clinopyroxene show variable fractionation patterns that have no correspondence between the two phases, which rules out sub-solidus re-equilibration (Matusiak-Malek et al., 2017). In addition, the lack of agreement between HFSE ratios of pyroxene phases and bulk rock melt depletion indicators imply either inherited source heterogeneity or melting followed by refertilization (Niu, 2004; Weyer et al., 2003). In contrast, bulk peridotite HFSE ratios are uniformly fractionated (Avg. Nb/Ta = 15.9 ± 0.8 ; Avg. $Zr/Hf = 43.6 \pm 1.4$), with absolute abundances of these elements being slightly depleted relative to primitive mantle. The clinopyroxene HFSE ratios are variable relative to the bulk peridotite or the gabbro. The variability within the clinopyroxenes and lack of correspondence with melt depletion suggest that interaction with low degree metasomatic melt and varying, partial re-equilibration occurred. Fractionation of the HFSE has been observed in other studies of abyssal peridotites and can be attributed to low degree partial melts from the asthenosphere (Niu, 2004).

5.3. The Extent and Timing of Melt-Depletion

A common characteristic of abyssal peridotites worldwide is a broad range of partial melt depletion that commonly exceeds 5% (Day et al., 2017; Harvey et al., 2006; Lassiter et al., 2014; Paquet et al., 2022; Warren, 2016). For example, abyssal peridotite suites from the Gakkel Ridge (4%–16%) (D'Errico et al., 2016), Mid-Atlantic (10%–14%) (Harvey et al., 2006), Southwest (2%–9%) and Central Indian (2%–12%) Ridges (Day et al., 2017) extend to >10% melt depletion, with the exception of the Southwest Indian Ridge. Two independent estimates of melt depletion using spinel compositions (Hellebrand et al., 2001) and HREE contents in whole-rock samples

OLLER ET AL. 6 of 15

| | MgO (wt.%) | Al_2O_3 (wt.%) | Olivine (Fo) | 2σ | F Spinel | Re | Pd | Pt | Ru | Ir | o | Pd/Ir | Ru/Ir | ¹⁸⁷ Re/ ¹⁸⁸ Os | 2σ | $\mathrm{SO}_{881}/\mathrm{SO}_{L81}$ | 2σ | $T_{RD} \\ (Ma)$ |
|------------|---------------|------------------|-----------------|------|-------------|-------|-------|-------|-------|-------|-------|-------|-------|--------------------------------------|--------|---------------------------------------|---------|------------------|
| WOBA 3D-1 | 46.2 | 1.1 | 91.6 | 0.1 | 15 | 0.017 | 1.06 | 2.73 | 8.31 | 4.84 | 7.15 | 0.56 | 1.16 | 0.0111 | 0.0002 | 0.11700 | 0.00006 | 1757 |
| WOBA 3D-3 | 41.1 | 2.4 | 8.68 | 0.04 | 8 | 0.257 | 5.99 | 5.76 | 5.84 | 3.26 | 2.84 | 1.77 | 2.06 | 0.4366 | 0.0065 | 0.13056 | 0.00006 | 1 |
| WOBA 3D-5 | 43.0 | 1.8 | 89.1 | 0.1 | 7 | 0.049 | 2.57 | 4.30 | 4.75 | 2.95 | 1.98 | 1.45 | 2.40 | 0.1192 | 0.0018 | 0.12208 | 0.00015 | 1054 |
| WOBA 3D-6 | 42.6 | 2.0 | 90.2 | 0.1 | 111 | 0.126 | 6.31 | 90.9 | 5.80 | 3.29 | 2.44 | 1.84 | 2.38 | 0.2492 | 0.0037 | 0.13261 | 0.00011 | , |
| WOBA 3D-7 | 42.5 | 2.3 | 8.68 | 0.1 | 8 | 0.118 | 09.9 | 6.03 | 6.25 | 3.19 | 2.73 | 1.89 | 2.29 | 0.2085 | 0.0031 | 0.12899 | 0.00011 | 98 |
| WOBA 3D-9 | 42.7 | 1.8 | 0.06 | 0.1 | 6 | 0.107 | 3.08 | 4.14 | 4.08 | 2.02 | 1.91 | 2.05 | 2.14 | 0.2695 | 0.0040 | 0.12590 | 0.00010 | 522 |
| WOBA 3D-10 | 45.3 | 2.0 | 89.0 | 4.2 | 10 | 0.026 | 2.27 | 5.20 | 3.67 | 1.67 | 1.37 | 3.12 | 2.68 | 0.0912 | 0.0014 | 0.12252 | 0.00070 | 993 |
| WOBA 3D-11 | 42.1 | 2.1 | 6.68 | 0.1 | 6 | 0.046 | 2.89 | 3.38 | 2.85 | 1.50 | 1.26 | 2.26 | 2.26 | 0.1773 | 0.0027 | 0.12981 | 0.00010 | 1 |
| WOBA 3D-12 | 44.0 | 1.5 | 90.1 | 0.1 | 11 | 0.088 | 5.54 | 5.19 | 5.04 | 2.91 | 2.31 | 1.78 | 2.18 | 0.1848 | 0.0028 | 0.12732 | 0.00015 | 321 |
| WOBA 3D-14 | 43.6 | 1.6 | 89.4 | 0.1 | 14 | 0.013 | 0.26 | 8.07 | 3.53 | 3.50 | 2.48 | 2.30 | 1.43 | 0.0262 | 0.0004 | 0.12256 | 0.00014 | 284 |
| WOBA 3D-15 | 42.8 | 2.1 | 90.2 | 0.1 | 111 | 0.085 | 5.25 | 99.7 | 7.07 | 3.99 | 3.02 | 1.92 | 2.34 | 0.1348 | 0.0020 | 0.12398 | 0.00008 | 790 |
| WOBA 3D-17 | 42.9 | 2.1 | 90.1 | 0.1 | 11 | 0.081 | 2.78 | 5.66 | 4.90 | 2.93 | 2.42 | 1.93 | 2.02 | 0.1615 | 0.0024 | 0.12599 | 0.00015 | 508 |
| WOBA 3D-31 | 43.6 | 1.7 | 90.1 | 0.1 | 8 | 0.032 | 5.71 | 99.7 | 5.18 | 2.43 | 2.13 | 3.15 | 2.43 | 0.0713 | 0.0011 | 0.12750 | 0.00008 | 297 |
| WOBA 3D-32 | 40.5 | 2.6 | 7.68 | 0.1 | 6 | 0.160 | 4.55 | 6.11 | 5.48 | 2.85 | 2.33 | 2.14 | 2.35 | 0.3310 | 0.0050 | 0.13071 | 0.00010 | ı |
| MUH-1 RED | n = 2 | | | | | 0.221 | 10.3 | 10.1 | 7.93 | 4.05 | 5.17 | | | | | 0.12644 | 0.00003 | |
| | 2σ | | | | | 0.001 | 0.266 | 2.144 | 0.593 | 699.0 | 1.069 | | | | | | | |
| OKUM RED | n = 2 | | | | | 0.538 | 12.5 | 11.0 | 4.66 | 0.98 | 0.71 | | | | | 0.2919 | 9900.0 | |
| | 2α | | | | | 0.008 | 0.003 | 0.044 | 0.010 | 0.061 | 0.034 | | | | | | | |

Note. TRD, Time of rhenium depletion age; calculated as: $1/\lambda \times \ln\{(1^{187} Os/^{188} Os_{chondrite} - ^{187} Os/^{188} Os_{sample})/[1^{187} Re/^{188} Os_{chondrite}]) + 1\}$. TRD ages are generally relevant only to strongly melt-depleted, refractory harzburgites and are included here solely as points of comparison.

15252027, 2022, 11, Downloaded from https://agupubs.onlinelibrary.wiley.com/doi/10.1029/2023CGO10353 by University Of California, Wiley Online Library on [1107/2024]. See the Terms and Conditions (https://onlinelibrary.wiley.com/terms-and-conditions) on Wiley Online Library for rules of use; OA articles are governed by the applicable Creative Commons License

15252027, 2022, 11, Downloaded from https://agupubs.onlinelibrary.wiley.com/doi/10.1029/2022GC010353 by University Of California, Wiley Online Library on [11/07/2024]. See the Terms and Condit

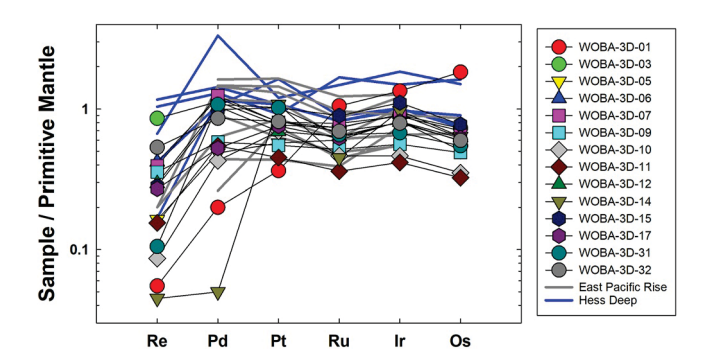


Figure 5. Primitive Mantle normalized highly siderophile element patterns for Ferrel Seamount peridotites, and published data from the East Pacific Rise (heavy gray lines) (Rehkämper et al., 1999; Snow & Schmidt, 1998) and Hess Deep (heavy blue lines) (Paquet et al., 2022). Primitive mantle composition is from Day et al. (2017).

(e.g., Johnson et al., 1990; Warren, 2016) yield between 7% to 15% and 6%–18% melt removal, respectively, indicating a similar degree of melt depletion in Ferrel peridotites relative to abyssal peridotites (Figure 6a).

Clinopyroxene is the primary reservoir of the REE in abyssal and continental peridotites, and as such the REE composition has been widely employed as a melt depletion indicator (Johnson et al., 1990). Nevertheless, we have demonstrated that the Ferrel peridotite clinopyroxene formed during melt refertilization during mid-ocean ridge processes and prior to the cryptic metasomatism affecting bulk rocks due to interaction with the host melt. Melt depletion calculations for the clinopyroxene indicate 4%–12% melt removal, agreeing well with the whole rock and spinel estimates. Despite the lack of correspondence between HFSE and melt depletion, these results suggest Ferrel peridotites are both residues after melt removal and have been refertilized with melts from similarly depleted sources.

The HSE are hosted in sulfide phases as opposed to silicate phases used for typical melt depletion indicators. Given the high abundance of the HSE in

peridotite relative to melts, bulk rock HSE abundances in peridotites preserve melt depletion signatures relatively robustly (F, Brandon et al., 2000; Day et al., 2017; Luguet et al., 2001; Paquet et al., 2022). To examine this for Ferrel peridotites, a non-modal batch melt model that tracks F as a function of (Pd/Ir)_N was used with parameters from Day et al. (2017), Luguet et al. (2003), and Liu et al. (2009) (Figure 8). This model assumes HSE control by sulfide-melt, which is exhausted at $F \ge 15\%$. The intent is to predict the degree of melt depletion where Pd/Ir ratios will be affected, not the specific ratio of Pd/Ir as this model does not account for pre-existing heterogeneity. As such, an exact fit to the model curves is not expected. The model agrees well with silicate melt-depletion models, showing sulfide removal in the range of 7%–15% F.

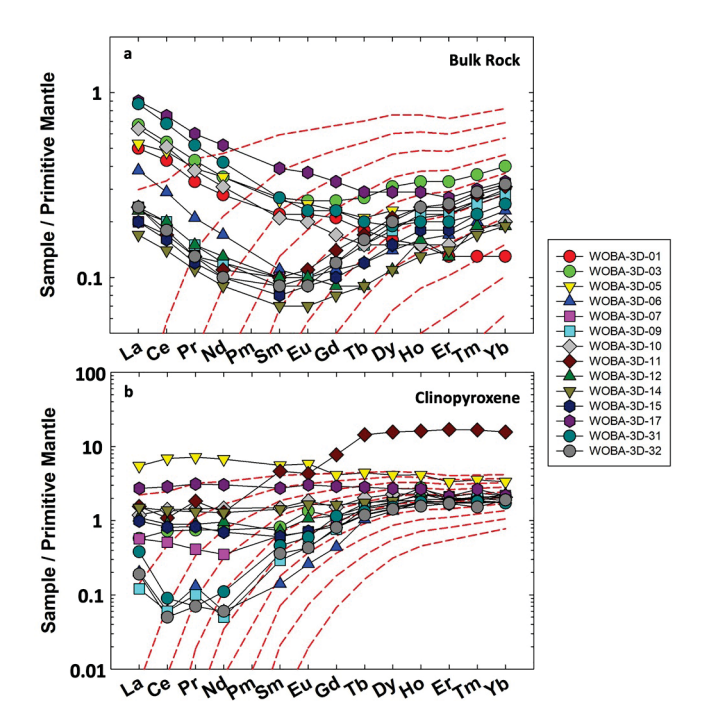


Figure 6. Primitive mantle normalized rare earth element patterns for Ferrel peridotites, (a) bulk rock, (b) average clinopyroxene. Red dashed lines indicate 2% melt increments (0%–18%) for non-modal fractional melt model. Model parameters from Warren (2016). Primitive mantle normalization from McDonough and Sun (1995).

5.4. Origin of Ferrel Seamount Peridotites From an Oceanic Lithosphere Protolith

Ferrel Seamount peridotites have physical, chemical, and isotopic characteristics suggesting that they are essentially identical to abyssal peridotites, with the exception that they have experienced recent cryptic metasomatism by alkali basalt partial melts and are generally fresher rocks. Otherwise, enrichments in whole rock LREE and other incompatible elements are characteristic features indicative of melt refertilization (Day et al., 2017; Niu, 2004; Warren, 2016), and Os isotopes, along with relative and absolute abundances of the HSE point to at least one ancient (hundreds of million years ago) melt depletion event with between 6% and 15% melt-loss, with strong similarities to East Pacific Rise abyssal peridotites.

Seamounts and volcanic islands within the Baja California margin have been interpreted as edifices emplaced atop of abandoned spreading centers (Batiza, 1977; Castillo et al., 2010). For example, geochemical studies of basalts dredged from the Davidson seamount have shown temporally variable fractionation, consistent with a shallow DMM source (Castillo et al., 2010; Davis et al., 2002). Seamounts along the California margin and California Borderlands (Guide, Pioneer, and Gumdrop seamounts), share similar characteristics to the Davidson seamount and those of the Baja California margin (Castillo et al., 2010; Davis et al., 2002). Perhaps most notable of these edifices is nearby Isla Guadalupe, for which Batiza (1977) drew a similar conclusion (Figure 1). Based on this evidence, we conclude that the Ferrel Seamount is a younger edifice emplaced atop an abandoned spreading section of the Pacific-Farallon ridge. In a detailed geomorphological, magnetic and seismic survey of the region, Lonsdale (1991) suggested that the Ferrel Seamount, and the Soledad rise to the north, defines the northern

OLLER ET AL. 8 of 15

15252027, 2022, 11, Downloaded from https://agupubs.onlinelibrary.wiley.com/doi/10.1029/2022GC010353 by University Of California, Wiley Online Library on [11/07/2024]. See the Terms

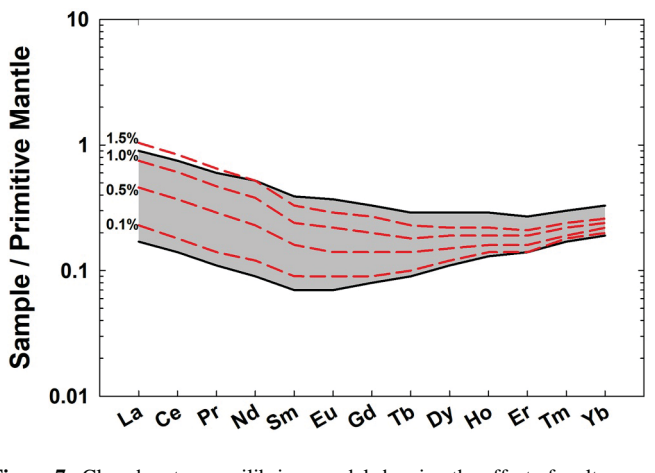


Figure 7. Closed system equilibrium model showing the effect of melt addition on LREE abundances. The initial composition is WOBA-3D-14. The gray field shows the Ferrel seamount peridotite samples from this study. The red dashed lines shows the effect of $\sim 0.1\%$, 0.5%, 1.0%, and 1.5% addition of the host alkali basalt on depleted peridotite.

are consistent with them being oceanic mantle lithosphere incorporated into the northwest boundary of the captured Guadalupe microplate.

and southern features of a mid-ocean ridge segment, referred to as the Soledad Ridge. The location of the peridotite xenoliths, and their compositions,

5.5. An "Isolation" Hypothesis for the Formation of Non-Cratonic CLM

The continental lithospheric mantle (CLM) is distinct in its thickness, and long-term stability compared to oceanic mantle lithosphere, as well as rigidity with regard to young lithosphere. Three models, outlined in the introduction, have previously been proposed to explain this distinction, all of which invoke substantial partial melting to render a buoyant, refractory residue that is difficult to subduct and recycle (Figure 9). The two models considered to occur after reduction in mantle potential temperatures in the Archean propose that buoyant slabs, of hotspot or volcanic arc origin, are accreted laterally or under-plated to the continental margin in subduction zones.

Here, we propose an alternative and complementary model that may be relevant to modern plate tectonics whereby subduction stalling, followed by ridge jump preserves a refractory oceanic slab, which can then be transposed and accreted to the margin by transpressive tectonic regimes, similar to processes

that formed the Canadian Cordillera (Samson & Patchett, 1991). Geophysical surveys, along with xenolith studies, indicate the non-cratonic continental margin of the western United States and Canada is ~100–150 km thick (Artemieva, 2009). Therefore, if fragments of oceanic lithosphere can evolve to non-cratonic CLM (especially relatively young, non-subducting lithosphere) the fragments must be thickened either through shortening from under thrusting, folding, or stacking. We envisage that a variety of other tectonically driven isolation processes

(e.g., rifting to isolate the plate) may also lead to formation of new CLM. Van den Broek & Gaina (2020) suggested that extension and rifting play an important role in the formation of microcontinents, and proposed southern Baja California to be a "proto-microcontinent". Here, we provide evidence for such a process on the Baja California margin. The Baja California margin approached its present-day state at ~15-10 Ma, when subduction ended, followed by the capture of the remaining Farallon micro-plates by the Pacific plate, and rifting inboard of the abandoned trench, which opened the Gulf of California (e.g., Atwater, 1970; Lonsdale, 1991). The result of this tectonic reorganization is a diffuse Pacific-North American plate boundary that incorporates many of the abandoned Pacific-Farallon spreading ridges, including the Soledad Ridge and associated Ferrel Seamount. The significance of ridge jump is that nascent oceanic lithosphere was isolated from subduction for at least 10 Ma. The Ferrel Seamount peridotites reveal that the lithosphere beneath is refractory material incorporated into the diffuse Pacific-North American plate boundary.

A modern analog for this sequence of events is the Colima basin southeast of the mouth of the Gulf of California proximal to the Rivera triple junction (Figure 10). Here, another Farallon remnant, the Rivera microplate is subducting beneath the northern most extent of the Middle America Trench at a decreasing rate over the last 2 Ma (G. T. Nixon, 1982). Detailed mapping, geochronology, and geochemical analysis by Luhr et al. (1985) suggests the Colima basin is an active rift inboard a waning subduction zone. These results imply subduction of the Rivera microplate will stall, inland rifting of the continental margin will continue, and the Rivera microplate along with a fragment of the North American plate will be captured and translated northward by the Pacific plate, preserving the underlying oceanic mantle lithosphere. In both cases of the Ferrel Seamount and Colima basin, oceanic

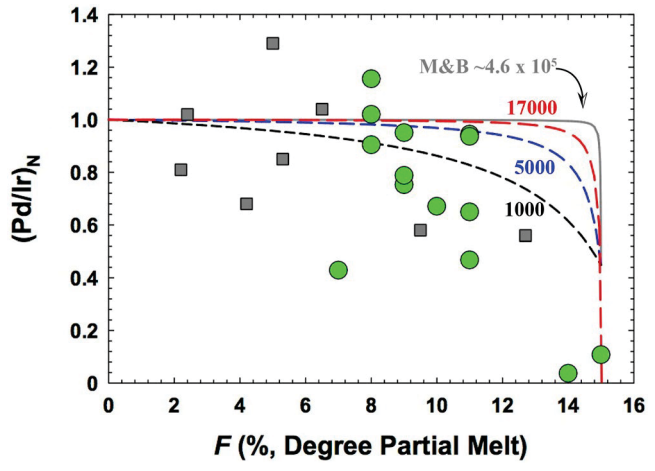


Figure 8. Primitive mantle normalized Pd/Ir melt model where F is obtained from Cr-spinel compositions (Hellebrand et al., 2001). Green circles are samples from this study; gray squares are SWIR (Day et al., 2017). This model predicts depletion of Pd/Ir from \sim 6 to 15% F; it is not intended to predict the trajectory of depletion. The initial Pd/Ir composition used is that of the primitive mantle. Curves represent Pd sulfide-silicate partition coefficients of 17,000, 5,000, and 1,000. The gray solid curve is the experimentally derived Kd (4.6 \pm 6.9 \times 10⁵) from Mungall and Brenan [2014]. A constant sulfide-silicate partition coefficient of 26,000 was used for Ir (Fleet et al., 1999). Initial conditions were set at 150 ppm S in a depleted mantle reservoir with a dissolved S of 1,000 ppm in melt. Under these conditions available sulfides in the residue are exhausted at F = 15% (Luguet et al., 2003).

OLLER ET AL. 9 of 15

and-conditions) on Wiley Online Library for rules of use; OA articles

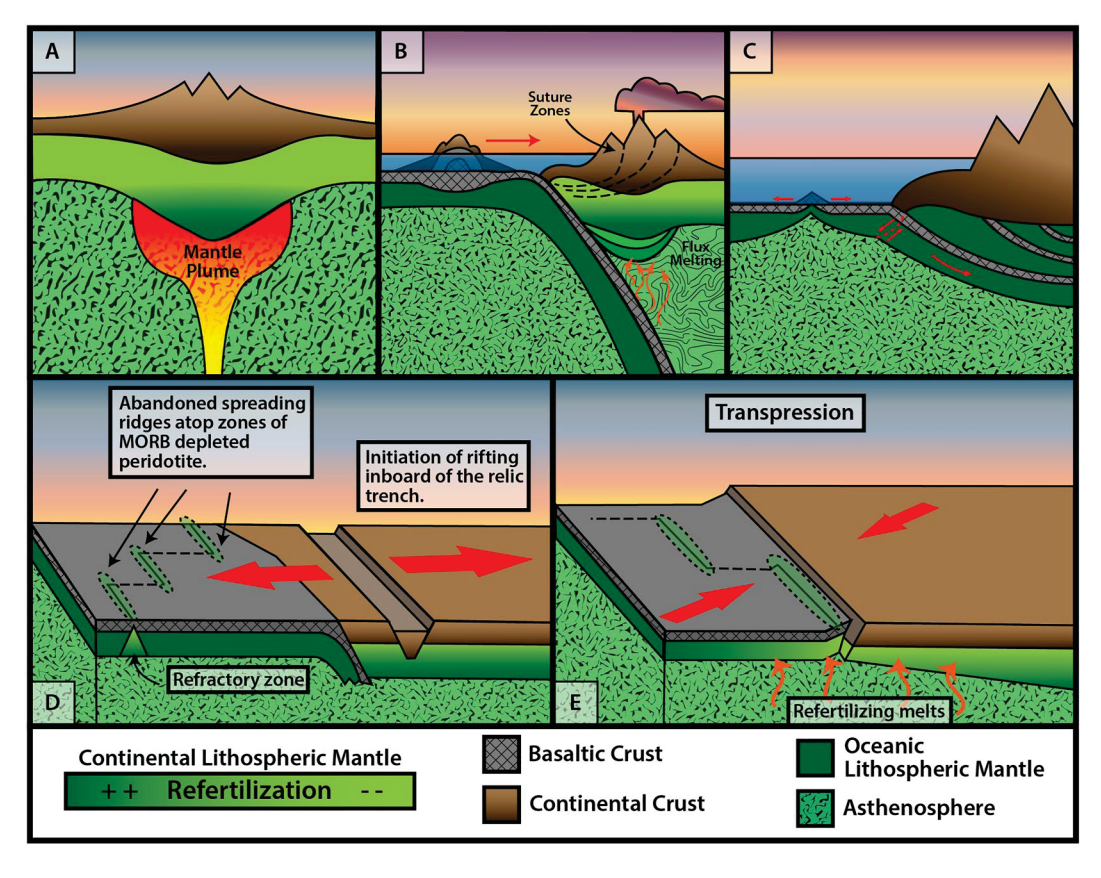


Figure 9. Schematic diagrams of mechanisms for formation of continental lithospheric mantle (a–c) and isolation of oceanic lithosphere and formation of nascent continental lithospheric mantle (d–e). (a) The plume model showing lithospheric thickening from prolonged melt depletion by a mantle plume (i.e., Griffin et al., 1998). (b) Exotic terrain accretion and lithospheric thickening from flux melting of the asthenosphere (Canil & Wei, 1992). (c) Imbrication of oceanic lithosphere from low angle subduction ("Subduction zone stacking"; i.e., Simon et al., 2008). (d) Model showing the isolation of refractory lithosphere by ridge jump, followed by (e) translation and accretion of the microplate in a transpressive environment (this study).

lithosphere is incorporated into the Pacific plate along with marginal non-cratonic CLM and eventually accreted to the margin, in contrast to previous models, which suggest buoyant oceanic lithosphere is directly accreted to a continental margin. The geochemical consequence of this process is that nascent CLM will have characteristics more akin to oceanic mantle lithosphere than to lithosphere involved in subduction processes, as in previous models for CLM formation. For example, comparing the Ferrel xenolith suite to other mantle xenolith suites from the Pacific (Snortum et al., 2019) shows the Ferrel Seamount shares the same range of ¹⁸⁷Os/¹⁸⁸Os and Os concentrations, consistent with a Pacific oceanic lithosphere origin (Figure 11).

5.6. Examining the Oceanic to Continental Lithospheric Mantle Model

The model of tectonic isolation to form CLM presented here suggests that refractory oceanic mantle lithosphere beneath the abandoned Pacific-Farallon spreading ridge has a higher probability of forming non-cratonic CLM due to chemical properties imparted by ridge processes coupled with tectonic reorganization through ridge jump. Therefore, an important question is whether CLM formation by isolation is a widespread process given the vast linear extent of subduction zones and mid ocean ridges worldwide. Although ridge subduction was initially thought to explain post Miocene volcanism along the North American margin, geophysical modeling and direct observation of abandoned ridge segments have cast doubt on this scenario (Michaud et al., 2006). Instead, as the hot, depleted ridge approaches the trench the angle of the subducting slab flattens and ultimately stalls prompting tectonic reorganization in the form of plate capture. These observations imply that oceanic lithosphere is not completely recycled, and rather that a limited fraction of the slab can be welded onto the plate. From this vantage

OLLER ET AL. 10 of 15

15252027, 2022, 11, Downloaded from https://agupubs.onlinelibrary.wiley.com/doi/10.1029/2022GC010353 by University Of California, Wiley Online Library on [11/07/2024]. See the Terms

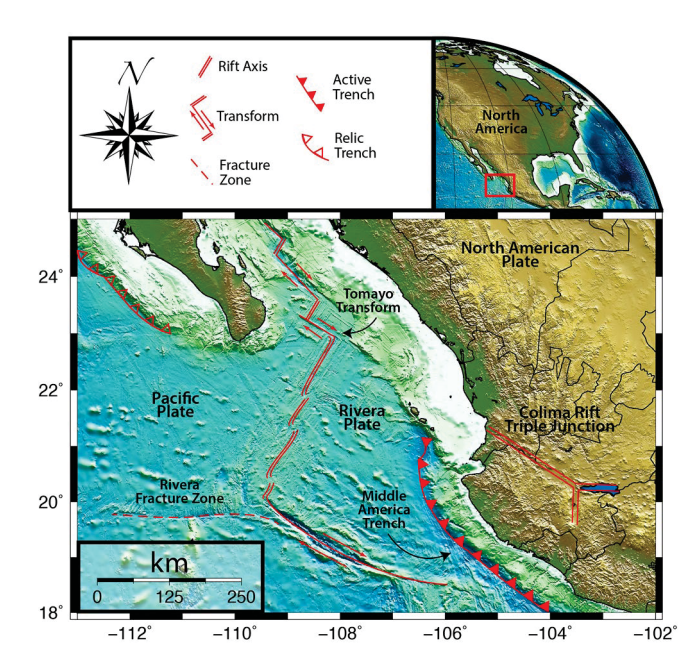


Figure 10. Elevation and bathymetry map of the Colima Rift in western Mexico near the southern point of Baja California. The Colima rift forms a triple junction structure where active spreading is advancing inland as subduction comes to a stop and spreading on the East Pacific Rise slows. This likely represents the transition of the North American-Pacific plate boundary and subsequent isolation of the Rivera section of the EPR.

point, the preserved lithosphere is accreted to the margin and oceanic lithosphere is imbricated against it (i.e., Luffi et al., 2009). This may be a major form of non-cratonic continental lithosphere formation.

Another question regards the role melt refertilization plays in the modification of oceanic lithosphere to CLM. Localities where non-cratonic CLM peridotites can be sampled in the western United States include Dish Hill and Kilbourne Hole, and these peridotite suites show evidence of more prolonged metasomatism than the Ferrel Seamount. Modal clinopyroxene for these CLM domains fall within the range of the Ferrel Seamount (3%-20%) but unlike peridotites from this study, the range of bulk rock Al₂O₃ for Dish Hill and Kilbourne Hole overlap fertile mantle values indicative of low degree metasomatism (Figure 12), implying the CLM becomes less stable with time due the addition of melt (i.e., Fe; Lee et al., 2011). Armytage et al. (2014) has suggested that the addition of refractory peridotite by under plating or partial melting shields the metasomatized lithosphere from further modification thus prolonging gravitational stability. This suggests a positive correlation between increasing degrees of melt depletion and depth. Where this theory implies vertical stacking of upper mantle domains as a result of subduction, our new model suggests isolated lithosphere can be added laterally in a strike-slip regime, broadly similar to the exotic terrain accretion model, in this case lacking the subduction component. Such a hypothesis works well with the ridge jump model proposed here in that continual tectonic processes gradually build CLM by lateral addition of refractory material along a diffuse transpressive boundary.

A comparison of ¹⁸⁷Os/¹⁸⁸Os and melt depletion indicators for Ferrel Seamount peridotites versus western United States xenolith suites indicates similar melt depletion processes consistent with previous studies that have

suggested an oceanic mantle lithosphere origin for Dish Hill (Luffi et al., 2009) and Rio Grande Rift xenoliths (Byerly & Lassiter, 2012). However, conclusive evidence linking abyssal peridotites to off-craton xenoliths is difficult due to post melt depletion modification by metasomatizing melts. This is illustrated in 187 Re- 187 Os ratios for Dish Hill and Kilbourne Hole samples that suggest elevated melt removal, similar to the Ferrel Seamount, but Al₂O₃ compositions that encompass the fertile mantle value (Figure 12).

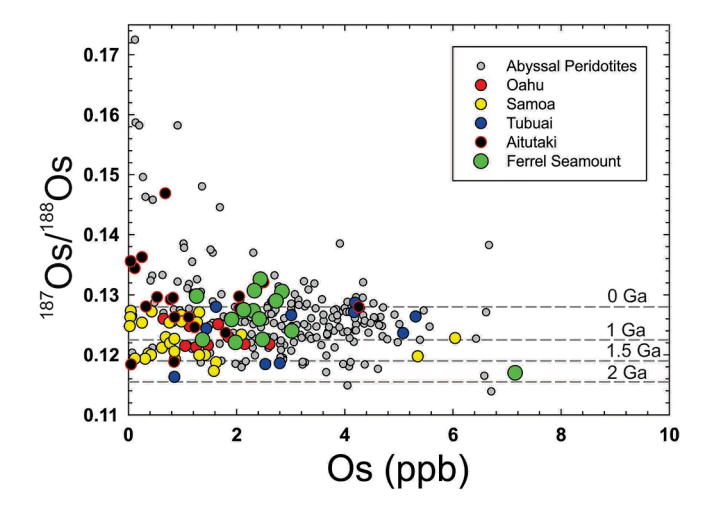


Figure 11. ¹⁸⁷Os/¹⁸⁸Os versus Os concentration for Ferrel Seamount xenoliths compared to Pacific island xenoliths representing ~75–100 Ma lithosphere and abyssal peridotites from around the globe. (Aitutaki: Snortum et al., 2019; Oahu, Hawaii: Bizimis et al., 2007; Samoa and Tubaii: Jackson et al., 2016; abyssal peridotites: Day et al., 2017).

6. Conclusions

Results for spinel peridotites dredged from the Ferrel Seamount indicate strong chemical, mineralogical, isotopic, and textural similarities to oceanic peridotites. The regional context of seafloor morphology indicates that the Ferrel Seamount is a post active spreading edifice situated atop an abandoned segment of the Pacific-Cocos Ridge system that likely samples preserved Pacific-Farralon lithosphere. Three independent melt models suggest the Ferrel samples experienced 8%-15% melt removal. Osmium isotopes indicate that most of this melt extraction occurred hundreds of millions of years before formation of this piece of oceanic lithosphere. At least one episode of refertilization is identified in the peridotite, preserved in clinopyroxene, occurring at the mid ocean ridge. This was followed by exposure of the peridotite xenoliths to low degree metasomatism, which imparted elevated LREE concentrations. Decoupling of melt depletion indicators and HFSE ratios of clinopyroxene versus bulk rock compositions support this conclusion. A model that tracks HSE behavior during partial melting support the results of Day et al. (2017) showing that HSE and Os isotopic systematics are not strongly leveraged by the effects of low degree melt rock reaction. These data lead to the framework of a new

OLLER ET AL.

15252027, 2022, 11, Downloaded from https://agupubs.onlinelibrary.wiley.com/doi/10.1029/2022GC010353 by University Of California, Wiley Online Library on [11/07/2024]. See the Terms and Conditions (https://onlinelibrary.wiley

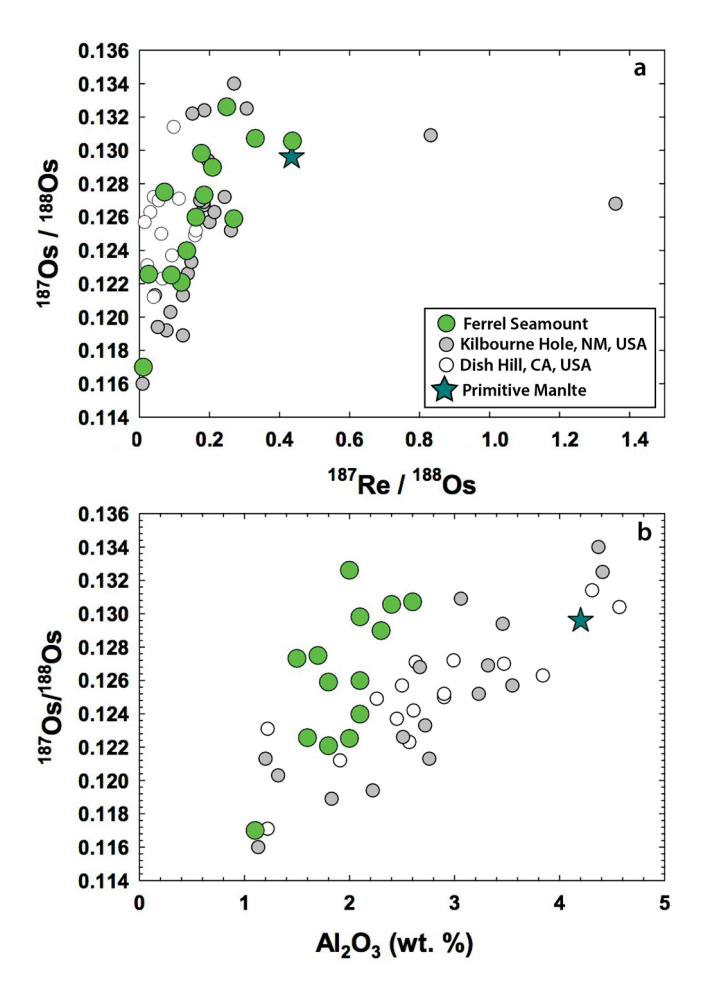


Figure 12. Plots of (a) ¹⁸⁷Re/¹⁸⁸Os-¹⁸⁷Os/¹⁸⁸Os for samples from the Ferrel Seamount, and Dish Hill, and Kilbourne Hole; (b) ¹⁸⁷Os/¹⁸⁸Os versus melt depletion indices, Al₂O₃. The CLM samples show a more fertile character, implying refertilization even in strongly melt-depleted samples. Primitive mantle value (PM—star) from Meisel et al. (2001).

model for the formation of CLM represented by non-cratonic xenoliths. We propose that tectonic reconfiguration, known as ridge jump, can isolate refractory and buoyant sections of lithosphere that may have experienced relatively recent melting. Hot and depleted in dense elements, lacking the force of slab pull, these sections of lithosphere are free to accrete to continental margins. During this time they may be exposed to prolonged addition and modification from highly variable degrees and compositions of refertilizing melt. Therefore, it seems necessary that further addition of refractory material to the base of the modified oceanic lithosphere is required to maintain gravitational stability over the 2 Ga time scales commonly reported for non-cratonic CLM xenolith suites.

Data Availability Statement

New data are available in the main manuscript and supplement. Data compilations used for comparisons for abyssal peridotites are from Snow and Schmidt (1998), Rehkämper et al. (1999), D'Errico et al. (2016), Warren (2016) (references therein), Day et al. (2017) (references therin) and Paquet et al. (2022). Pacific lithosphere data is from Bizimis et al., 2007; Jackson et al., 2016; Snortum et al., 2019. Western United States non-cratonic CLM data is from Harvey et al., 2012; Armytage et al., 2014. Maps were made using Generic Mapping Tools version 5.0 (https://www.genericmapping-tools.org/) (Wessel et al., 2013). Plots were made using SigmaPlot version 14.0 (https://systatsoftware.com/sigmaplot/).

OLLER ET AL. 12 of 15

15252027, 2022, 11, Downloaded from https://agupubs.onlinelibrary.wiley.

com/doi/10.1029/2022GC010353 by University Of California,

Wiley Online Library on [11/07/2024]. See the Terms

Geochemistry, Geophysics, Geosystems

Acknowledgments

The work would not have been possible without the support of our colleague, L. A. Taylor (1938–2017). We are grateful to L. Reisberg, A. Stracke and an anonymous reviewer for constructive journal review comments. D. van Acken and L. Ackerman are also thanked for comments on a previous version of the manuscript. Financial support from the National Science Foundation (Grants EAR 1447130 and EAR 1918322) is gratefully acknowledged. We thank the WOBA cruise participants, but especially B. Peters for selection and initial preparation of samples.

References

- Albarède, F. (1995). Introduction to geochemical modeling. Cambridge University Press. https://doi.org/10.1017/CBO9780511622960
- Armytage, R. M. G., Brandon, A. D., Peslier, A. H., & Lapen, T. J. (2014). Osmium isotope evidence for Early to Middle Proterozoic mantle lithosphere stabilization and concomitant production of juvenile crust in Dish Hill, CA peridotite xenoliths. *Geochimica et Cosmochimica Acta*, 137, 113–133. https://doi.org/10.1016/j.gca.2014.04.017
- Artemieva, I. M. (2009). The continental lithosphere: Reconciling thermal, seismic, and petrologic data. *Lithos*, 109(1–2), 23–46. https://doi.org/10.1016/j.lithos.2008.09.015
- Atwater, T. (1970). Implications of plate tectonics for the Cenozoic tectonic evolution of western North America. The Geological Society of America Bulletin, 81(12), 3513. https://doi.org/10.1130/0016-7606(1970)81[3513:ioptft]2.0.co;2
- Batiza, R. (1977). Petrology and chemistry of Guadalupe Island: An alkalic seamount on a fossil ridge crest. Geology, 5(12), 760–764. https://doi.org/10.1130/0091-7613(1977)5<760:pacogi>2.0.co;2
- Bizimis, M., Griselin, M., Lassiter, J. C., Salters, V. J., & Sen, G. (2007). Ancient recycled mantle lithosphere in the Hawaiian plume: Osmium-hafnium isotopic evidence from peridotite mantle xenoliths. *Earth and Planetary Science Letters*, 257(1–2), 259–273. https://doi.org/10.1016/j.epsl.2007.02.036
- Boyd, F. R. (1989). Compositional distinction between oceanic and cratonic lithosphere. Earth and Planetary Science Letters, 96(1–2), 15–26. https://doi.org/10.1016/0012-821X(89)90120-9
- Brandon, A. D., Snow, J. E., Walker, R. J., Morgan, J. W., & Mock, T. D. (2000). ¹⁹⁰Pt⁻¹⁸⁶Os and ¹⁸⁷Re⁻¹⁸⁷Os systematics of abyssal peridotites. Earth and Planetary Science Letters, 177(3-4), 319–335. https://doi.org/10.1016/S0012-821X(00)00044-3
- Brey, G. P., & Köhler, T. (1990). Geothermobarometry in four-phase lherzolites II. New thermobarometers, and practical assessment of existing thermobarometers. *Journal of Petrology*, 31(6), 1353–1378. https://doi.org/10.1093/petrology/31.6.1353
- Byerly, B. L., & Lassiter, J. C. (2012). Evidence from mantle xenoliths for lithosphere removal beneath the central Rio Grande Rift. Earth and Planetary Science Letters, 355–356, 82–93. https://doi.org/10.1016/j.epsl.2012.08.034
- Canil, D. (2004). Mildly incompatible elements in peridotites and the origins of mantle lithosphere. Lithos, 77(1-4), 375-393. https://doi.org/10.1016/j.lithos.2004.04.014
- Canil, D., & Wei, K. (1992). Constraints on the origin of mantle-derived low Ca garnets. Contributions to Mineralogy and Petrology, 109(4), 421–430. https://doi.org/10.1007/BF00306546
- Castillo, P. R., Clague, D. A., Davis, A. S., & Lonsdale, P. F. (2010). Petrogenesis of Davidson Seamount lavas and its implications for fossil spreading center and intraplate magmatism in the eastern Pacific. Geochemistry, 11(2). https://doi.org/10.1029/2009GC002992
- Choi, S. H., Shervais, J. W., & Mukasa, S. B. (2008). Supra-subduction and abyssal mantle peridotites of the Coast Range ophiolite, California. Contributions to Mineralogy and Petrology, 156(5), 551–576. https://doi.org/10.1007/s00410-008-0300-6
- Davis, A. S., Clague, D. A., Bohrson, W. A., Dalrymple, G. B., & Greene, H. G. (2002). Seamounts at the continental margin of California: A different kind of oceanic intraplate volcanism. GSA Bulletin, 114(3), 316–333. https://doi.org/10.1130/0016-7606(2002)114<0316:satcmo>2.0.co;2
- Day, J. M. D., Walker, R. J., & Warren, J. M. (2017). ¹⁸⁶Os-¹⁸⁷Os and highly siderophile element abundance systematics of the mantle revealed by abyssal peridotites and Os-rich alloys. *Geochimica et Cosmochimica Acta*, 200, 232–254. https://doi.org/10.1016/j.gca.2016.12.013
- D'Errico, M. E., Warren, J. M., & Godard, M. (2016). Evidence for chemically heterogeneous Arctic mantle beneath the Gakkel Ridge. Geochimica et Cosmochimica Acta, 174, 291–312. https://doi.org/10.1016/j.gca.2015.11.017
- Fleet, M. E., Crocket, J. H., Liu, M., & Stone, W. E. (1999). Laboratory partitioning of platinum-group elements (PGE) and gold with application to magmatic sulfide–PGE deposits. *Lithos*, 47(1–2), 127–142. https://doi.org/10.1016/S0024-4937(99)00011-0
- Frey, F. A., & Green, D. H. (1974). The minerology, geochemistry and origin of lherzolite inclusions in Victorian bassanites. *Geochimica et Cosmochimica Acta*, 38(7), 1023–1059. https://doi.org/10.1016/0016-7037(74)90003-9
- Frey, F. A., & Prinz, M. (1978). Ultramafic inclusions from San Carlos, Arizona: Pertrologic and geochemical data bearing on their petrogenesis. Earth and Planetary Science Letters, 38(1), 129–176. https://doi.org/10.1016/0012-821x(78)90130-9
- Galer, S., & O'Nions, R. K. (1989). Chemical and isotopic studies of ultramafic inclusions from the San Carlos Volcanic Field, Arizona: A bearing on their petrogenesis. *Journal of Petrology*, 30(4), 1033–1064. https://doi.org/10.1093/petrology/30.4.1033
- Griffin, W. L., OReilly, S. Y., Ryan, C. G., Gaul, O., & Ionov, D. A. (1998). Secular variation in the composition of subcontinental lithospheric mantle: Geophysical and geodynamic implications. *Geodynamics*, 26, 1–26.
- Harvey, J., Gannoun, A., Burton, K. W., Rogers, N. W., Alard, O., & Parkinson, I. J. (2006). Ancient melt extraction from the oceanic upper mantle revealed by Re-Os isotopes in abyssal peridotites from the Mid-Atlantic ridge. *Earth and Planetary Science Letters*, 244(3-4), 606-621. https://doi.org/10.1016/j.epsl.2006.02.031
- Harvey, J., Yoshikawa, M., Hammond, S. J., & Burton, K. W. (2012). Deciphering the trace element characteristics in Kilbourne Hole peridotite xenoliths: Melt–rock interaction and metasomatism beneath the Rio Grande Rift, SW USA. *Journal of Petrology*, *53*(8), 1709–1742. https://doi.org/10.1093/patrelogy/ags030.
- Hellebrand, E. (2002). Garnet-field melting and late-stage refertilization in "residual" abyssal peridotites from the Central Indian Ridge. *Journal of Petrology*, 43(12), 2305–2338. https://doi.org/10.1093/petrology/43.12.2305
- Hellebrand, E., Snow, J. E., Dick, H. J. B., & Hofmann, A. W. (2001). Coupled major and trace elements as indicators of the extent of melting in mid-ocean-ridge peridotites. *Nature*, 410(6829), 677–681. https://doi.org/10.1038/35070546
- Herzberg, C. (2004). Geodynamic information in peridotite petrology. *Journal of Petrology*, 45(12), 2507–2530. https://doi.org/10.1093/petrology/egh039
- Jackson, M. G., Shirey, S. B., Hauri, E. H., Kurz, M. D., & Rizo, H. (2016). Peridotite xenoliths from the Polynesian Austral and Samoa hotspots: Implications for the destruction of ancient ¹⁸⁷Os and ¹⁴²Nd isotopic domains and the preservation of Hadean ¹²⁹Xe in the modern convecting mantle. *Geochimica et Cosmochimica Acta*, 185, 21–43. https://doi.org/10.1016/j.gca.2016.02.011
- Jagoutz, E. (1988). Nd and Sr systematics in an eclogite xenolith from Tanzania: Evidence for frozen mineral equilibria in the continental lithosphere. Geochimica et Cosmochimica Acta, 52(5), 1285–1293. https://doi.org/10.1016/0016-7037(88)90282-7
- Jagoutz, E., Palme, H., Baddenhausen, H., Blum, K., Cendales, M., Dreibus, G., et al. (1979). The abundance of major, minor and trace elements in the Earth's mantle as derived from primitive ultramafic nodules. In *Proceedings of Lunar and Planetary Science Conference* (pp. 2031–2050).
- Jochum, K. P., Nohl, U., Herwig, K., Lammel, E., Stoll, B., & Hofmann, A. W. (2005). GeoReM: A new geochemical database for reference materials and isotopic standards. Geostandards and Geoanalytical Research, 29(3), 333–338. https://doi.org/10.1111/j.1751-908x.2005.tb00904.x
- Johnson, K. T. M., Dick, H. J. B., & Shimizu, N. (1990). Melting in the oceanic upper mantle: An ion microprobe study of diopsides in abyssal peridotites. *Journal of Geophysical Research*, 95(B3), 2661–2678. https://doi.org/10.1029/JB095iB03p02661

OLLER ET AL. 13 of 15

onlinelibrary.wiley.com/doi/10.1029/2022GC010353 by University Of California, Wiley Online Library on [11/07/2024]. See the Terms

Geochemistry, Geophysics, Geosystems

- Lassiter, J. C., Byerly, B. L., Snow, J. E., & Hellebrand, E. (2014). Constraints from Os-isotope variations on the origin of Lena Trough abyssal peridotites and implications for the composition and evolution of the depleted upper mantle. Earth and Planetary Science Letters, 403, 178–187. https://doi.org/10.1016/j.epsl.2014.05.033
- Lee, C.-T. A. (2006). Geochemical/petrologic constraints on the origin of cratonic mantle. Geophysical Monograph-American Geophysical Union, 164, 89.
- Lee, C. T. A., Luffi, P., & Chin, E. J. (2011). Building and destroying continental mantle. Annual Review of Earth and Planetary Sciences, 39(1), 59–90. https://doi.org/10.1146/annurev-earth-040610-133505
- Liu, C.-Z., Snow, J. E., Brügmann, G., Hellebrand, E., & Hofmann, A. W. (2009). Non-chondritic HSE budget in Earth's upper mantle evidenced by abyssal peridotites from Gakkel ridge (Arctic Ocean). Earth and Planetary Science Letters, 283(1–4), 122–132. https://doi.org/10.1016/j. epsl.2009.04.002
- Lonsdale, P. (1991). Structural patterns of the Pacific floor offshore of penisular California. AAPG Memoir, 47, 87–125.
- Luffi, P., Saleeby, J. B., Lee, C. T. A., & Ducea, M. N. (2009). Lithospheric mantle duplex beneath the central Mojave Desert revealed by xeno-liths from Dish Hill, California. *Journal of Geophysical Research*, 114(B3), 375. https://doi.org/10.1029/2008JB005906
- Luguet, A., Alard, O., Lorand, J. P., Pearson, N. J., Ryan, C., & O'Reilly, S. Y. (2001). Laser-ablation microprobe (LAM)-ICPMS unravels the highly siderophile element geochemistry of the oceanic mantle. Earth and Planetary Science Letters, 189(3-4), 285-294. https://doi. org/10.1016/S0012-821X(01)00357-0
- Luguet, A., Lorand, J.-P., & Seyler, M. (2003). Sulfide petrology and highly siderophile element geochemistry of abyssal peridotites: A coupled study of samples from the Kane Fracture Zone (45°W 23°20N, MARK area, Atlantic Ocean). Geochimica et Cosmochimica Acta, 67(8), 1553–1570. https://doi.org/10.1016/S0016-7037(02)01133-X
- Luguet, A., & Pearson, G. (2019). Dating mantle peridotites using Re-Os isotopes: The complex message from whole rocks, base metal sulfides, and platinum group minerals. American Minerologist: Journal of Earth and Planetary Materials, 104(2), 165–189. https://doi.org/10.2138/am-2019-6557
- Luguet, A., & Reisberg, L. (2016). Highly siderophile element and ¹⁸⁷Os signatures in non-cratonic basalt-hosted peridotite xenoliths: Unravelling the origin and evolution of the post-Archean lithospheric mantle. *Reviews in Mineralogy and Geochemistry*, 81(1), 305–367. https://doi.org/10.2138/rmg.2016.81.06
- Luhr, J. F., Nelson, S. A., Allan, J. F., & Carmichael, I. S. E. (1985). Active rifting in southwestern Mexico: Manifestations of an incipient eastward spreading-ridge jump. *Geology*, 13(1), 54–57. https://doi.org/10.1130/0091-7613(1985)13<54:arismm>2.0.co;2
- Mallick, S., Dick, H. J., Sachi-Kocher, A., & Salters, V. J. (2014). Isotope and trace element insights into heterogeneity of subridge mantle. Geochemistry, Geophysics, Geosystems, 15(6), 2438–2453. https://doi.org/10.1002/2014gc005314
- Matusiak-Małek, M., Puziewicz, J., Ntaflos, T., Grégoire, M., Kukuła, A., & Wojtulek, P. M. (2017). Origin and evolution of rare amphibole-bearing mantle peridotites from Wilcza Góra (SW Poland), Central Europe. *Lithos*, 286–287, 302–323. https://doi.org/10.1016/j.lithos.2017.06.017
- McDonough, W. F., & Sun, S.-S. (1995). The composition of the Earth. Chemical Geology, 120(3-4), 223-253. https://doi.org/10.1016/0009-2541(94)00140-4
- Meisel, T., Walker, R. J., Irving, A. J., & Lorand, J.-P. (2001). Osmium isotopic compositions of mantle xenoliths: A global perspective. Geochimica et Cosmochimica Acta, 65(8), 1311–1323. https://doi.org/10.1016/S0016-7037(00)00566-4
- Michaud, F., Royer, J. Y., Bourgois, J., Dyment, J., Calmus, T., Bandy, W., et al. (2006). Oceanic-ridge subduction vs. slab break off: Plate tectonic evolution along the Baja California Sur continental margin since 15 Ma. *Geology*, 34(1), 13. https://doi.org/10.1130/g22050.1
- Müller, R. D., Sdrolias, M., Gaina, C., & Roest, W. R. (2008). Age, spreading rates, and spreading asymmetry of the world's ocean crust. *Geochemistry*, 9(4), Q04006. https://doi.org/10.1029/2007GC001743
- Mungall, J. E., & Brenan, J. M. (2014). Partitioning of platinum-group elements and Au between sulfide liquid and basalt and the origins of mantle-crust fractionation of the chalcophile elements. *Geochimica et Cosmochimica Acta*, 125, 265–289. https://doi.org/10.1016/j.gca.2013.10.002
- Nisbet, E. G., Cheadle, M. J., Arndt, N. T., & Bickle, M. J. (1993). Constraining the potential temperature of the Archaean mantle: A review of the evidence from komatiites. *Lithos*, 30(3–4), 291–307. https://doi.org/10.1016/0024-4937(93)90042-B
- Niu, Y. (2004). Bulk-rock major and trace element compositions of abyssal peridotites: Implications for mantle melting, melt extraction and post-melting processes beneath mid-ocean ridges. *Journal of Petrology*, 45(12), 2423–2458. https://doi.org/10.1093/petrology/egh068
- Niu, Y., & O'Hara, M. J. (2003). Origin of ocean island basalts: A new perspective from petrology, geochemistry, and mineral physics considerations. *Journal of Geophysical Research*, 108(B4), 2209. https://doi.org/10.1029/2002JB002048
- Nixon, G. T. (1982). The relationship between Quaternary volcanism in central Mexico and the seismicity and structure of subducted ocean lithosphere. *The Geological Society of America Bulletin*, 93(6), 514–523. https://doi.org/10.1130/0016-7606(1982)93<514:trbqvi>2.0.co;2 Nixon, P. N. (1987). Mantle xenolith perspectives. *Mantle Xenoliths*, 96(3), 741–756.
- Paquet, M., Day, J. M. D., Brown, D. B., & Waters, C. L. (2022). Effective global mixing of the highly siderophile elements into Earth's mantle inferred from oceanic abyssal peridotites. *Geochimica et Cosmochimica Acta*, 316, 347–362. https://doi.org/10.1016/j.gca.2021.09.033
- Pearce, J. A., & Parkinson, I. J. (1993). Trace element models for mantle melting: Application to volcanic arc petrogenesis. *Geological Society*, London, Special Publications, 76(1), 373–403. https://doi.org/10.1144/GSL.SP.1993.076.01.19
- Pearson, D. G., Canil, D., & Shirey, S. B. (2004). Mantle samples included in volcanic rocks: Xenoliths and diamonds. *Treatise on geochemistry*, 2, 568.
- Pearson, D. G., Carlson, R. W., Shirey, S. B., Boyd, F. R., & Nixon, P. H. (1995). Stabilisation of Archaean lithospheric mantle: A ReOs isotope study of peridotite xenoliths from the Kaapvaal craton. *Earth and Planetary Science Letters*, 134(3–4), 341–357. https://doi.org/10.1016/0012-821X(95)00125-V
- Pearson, D. G., Scott, J. M., Liu, J., Schaeffer, A., Wang, L. H., van Hunen, J., et al. (2021). Deep continental roots and cratons. *Nature*, 596(7871), 199–210. https://doi.org/10.1038/s41586-021-03600-5
- Pearson, D. G., & Wittig, N. (2008). Formation of Archaean continental lithosphere and its diamonds: The root of the problem. *Journal of the Geological Society*, 165(5), 895–914. https://doi.org/10.1144/0016-76492008-003
- Peslier, A. H., Reisberg, L., Ludden, J., & Francis, D. (2000). Os isotopic systematics in mantle xenoliths; age constraints on the Canadian Cordillera lithosphere. Chemical Geology, 166(1–2), 85–101. https://doi.org/10.1016/s0009-2541(99)00187-4
- Pfänder, J. A., Münker, C., Stracke, A., & Mezger, K. (2007). Nb/Ta and Zr/Hf in ocean island basalts Implications for crust–mantle differentiation and the fate of Niobium. Earth and Planetary Science Letters, 254(1–2), 158–172. https://doi.org/10.1016/j.epsl.2006.11.027
- Rehkämper, M., Halliday, A. N., Fitton, J. G., Lee, D. C., Wieneke, M., & Arndt, N. T. (1999). Ir, Ru, Pt, and Pd in basalts and komatiites: New constraints for the geochemical behavior of the platinum-group elements in the mantle. *Geochimica et Cosmochimica Acta*, 63(22), 3915–3934. https://doi.org/10.1016/S0016-7037(99)00219-7

OLLER ET AL. 14 of 15

- Rudnick, R. L., McDonough, W. F., & Chappell, B. W. (1993). Carbonatite metasomatism in the northern Tanzanian mantle: Petrographic and geochemical characteristics. *Earth and Planetary Science Letters*, 114(4), 463–475. https://doi.org/10.1016/0012-821X(93)90076-L
- Samson, S. D., & Patchett, P. J. (1991). The Canadian Cordillera as a modern analogue of Proterozoic crustal growth. Australian Journal of Earth Sciences, 38(5), 595–611. https://doi.org/10.1080/08120099108727994
- Schulze, D. J. (1986). Calcium anomalies in the mantle and a subducted metaserpentinite origin for diamonds. *Nature*, 319(6053), 483–485. https://doi.org/10.1038/319483a0
- Shirey, S. B., & Richardson, S. H. (2011). Start of the Wilson cycle at 3 Ga shown by diamonds from subcontinental mantle. *Science*, 333(6041), 434–436. https://doi.org/10.1126/science.1206275
- Simon, N. S. C., Neumann, E.-R., Bonadiman, C., Coltorti, M., Delpech, G., Grégoire, M., & Widom, E. (2008). Ultra-refractory domains in the oceanic mantle lithosphere sampled as mantle xenoliths at ocean islands. *Journal of Petrology*, 49(6), 1223–1251. https://doi.org/10.1093/petrology/egn023
- Snortum, E., & Day, J. M. D. (2020). Forearc origin for Coast Range Ophiolites inferred from osmium isotopes and highly siderophile elements. Chemical Geology, 550, 119723. https://doi.org/10.1016/j.chemgeo.2020.119723
- Snortum, E., Day, J. M. D., & Jackson, M. G. (2019). Pacific Lithosphere evolution inferred from Aitutaki mantle xenoliths. *Journal of Petrology*, 60(9), 1753–1772. https://doi.org/10.1093/petrology/egz047
- Snow, J. E., & Schmidt, G. (1998). Constraints on Earth accretion deduced from noble metals in the oceanic mantle. *Nature*, 391(6663), 166–169. https://doi.org/10.1038/34396
- Stern, R. J. (2002). Subduction zones. Reviews of Geophysics, 40(4), 3-1-3-38. https://doi.org/10.1029/2001RG000108
- van den Broek, J. M., & Gaina, C. (2020). Microcontinents and continental fragments associated with subduction systems. *Tectonics*, 39(8), e2020TC006063. https://doi.org/10.1029/2020TC006063
- Warren, J. M. (2016). Global variations in abyssal peridotite compositions. Lithos, 248–251, 193–219. https://doi.org/10.1016/j.lithos.2015.12.023
 Wessel, P., Smith, W. H. F., Scharroo, R., Luis, J., & Wobbe, F. (2013). Generic mapping tools: Improved version released. Eos, Transactions
 American Geophysical Union, 94(45), 409. https://doi.org/10.1029/98eo00426
- Weyer, S., Münker, C., & Mezger, K. (2003). Nb/Ta, Zr/Hf and REE in the depleted mantle: Implications for the differentiation history of the crust–mantle system. Earth and Planetary Science Letters, 205(3–4), 309–324. https://doi.org/10.1016/S0012-821X(02)01059-2
- Workman, R. K., & Hart, S. R. (2005). Major and trace element composition of the depleted MORB mantle (DMM). Earth and Planetary Science Letters, 231(1–2), 53–72. https://doi.org/10.1016/j.epsl.2004.12.005

References From the Supporting Information

- Boyd, F. R., & Mertzman, S. A. (1987). Composition and structure of the Kaapvaal lithosphere, southern Africa, magmatic processes: Physicochemical principles. BO Mysen.
- Birck, J. L., Barman, M. R., & Campas, F. (1997). Re-Os isotopic measurments at the femtomole level in natural samples. *Geostandards Newslatter*, 21(1), 19-27
- Creaser, R. A., Papanastassiou, D. A., & Wasserburg, G. J. (1991). Negative thermal ion mass spectrometry of osmium, rhenium amd iridium. Geochimica et Cosmochimica Acta, 55(1), 397–401. https://doi.org/10.1016/0016-7037(91)90427-7
- Day, J. M. D., Peters, B. J., & Janney, P. E. (2014). Oxygen isotope systematics of South African olivine melilitites and implications for HIMU mantle reservoirs. *Lithos*, 202–203, 76–84. https://doi.org/10.1016/j.lithos.2014.05.009
- Day, J. M. D., Waters, C. L., Schaefer, B. F., Walker, R. J., & Turner, S. (2016). Use of hydrofluoric acid desilicification in the determination of highly siderophile element abundances and Re-Pt-Os isotope systematics in mafic-ultramafic rocks. *Geostandards and Geoanalytical Research*, 40(1), 49–65. https://doi.org/10.1111/j.1751-908x.2015.00367.x
- Volkening, J., Walczyk, T., & Heumann, K. G. (1991). Osmium isotope ratio determinations by negative thermal ionization mass spectrometry. International Journal of Mass Spectrometry and Ion Processes, 105(2), 147–159. https://doi.org/10.1016/0168-1176(91)80077-z
- Zhou, M.-F., Robinson, P. T., Malpas, J., & Li, Z. (1996). Podiform chromitites in the Luobusa ophiolite (southern Tibet): Implications for melt-rock interaction and chromite segregation in the upper mantle. *Journal of Petrology*, 37(1), 3–21. https://doi.org/10.1093/petrology/37.1.3

OLLER ET AL. 15 of 15